DOI: 10.1002/cmdc.201000332

Modeling and Biological Investigations of an Unusual Behavior of Novel Synthesized Acridine-Based Polyamine Ligands in the Binding of Double Helix and G-Quadruplex DNA

Carla Bazzicalupi,*[a] Matteo Chioccioli,[b] Claudia Sissi,*[c] Elena Porcù,[c] Claudia Bonaccini,[b] Claudia Pivetta,[c] Andrea Bencini,[a] Claudia Giorgi,[a] Barbara Valtancoli,[a] Fabrizio Melani,[b] and Paola Gratteri*[b]

Three novel 2,7-substituted acridine derivatives were designed and synthesized to investigate the effect of this functionalization on their interaction with double-stranded and G-quadruplex DNA. Detailed investigations of their ability to bind both forms of DNA were carried out by using spectrophotometric, electrophoretic, and computational approaches. The ligands in this study are characterized by an open-chain (L1) or a macrocyclic (L2, L3) framework. The aliphatic amine groups in the macrocycles are joined by ethylene (L2) or propylene chains (L3). L1 behaved similarly to the lead compound *m*-AMSA, efficiently intercalating into dsDNA, but stabilizing G-quadruplex structures poorly, probably due to the modest stabilization effect exerted by its protonated polyamine chains. L2 and L3, containing small polyamine macrocyclic frameworks, are known to adopt a rather bent and rigid conformation; thus they are generally expected to be sterically impeded from recognizing dsDNA according to an intercalative binding mode. This was confirmed to be true for L3. Nevertheless, we show that L2 can give rise to efficient π–π and H-bonding interactions with dsDNA. Additionally, stacking interactions allowed L2 to stabilize the G-quadruplex structure: using the human telomeric sequence, we observed the preferential induction of tetrameric G-quadruplex forms. Thus, the presence of short ethylene spacers seems to be essential for obtaining a correct match between the binding sites of L2 and the nucleobases on both DNA forms investigated. Furthermore, current modeling methodologies, including docking and MD simulations and free energy calculations, provide structural evidence of an interaction mode for L2 that is different from that of L3; this could explain the unusual stabilizing ability of the ligands (L2 > L3 > L1) toward G-quadruplex that was observed in this study.

Introduction

The activity of many antimalarial, antibacterial, and anticancer agents is based on their interaction with helical double-stranded DNA (dsDNA).[1–3] As a consequence, much effort has been devoted over the past few decades to the design and synthesis of new molecules that can reversibly bind and/or react with dsDNA; the aim of these research efforts has been to use these compounds as novel drugs or as probes to better understand the mechanism of action of drugs that are already available.

More recently, interest has also focused on non-canonical DNA structures. For example, a great deal of attention has been devoted to clarifying the structural features of telomeric DNA.[4–8] In fact, the telomeric sequence has been found to be closely related to the immortalization process of cancer cells[9–14] and genetic stability.[15–17] Therefore, it represents a potentially suitable target for anticancer therapy. Telomeres consist of guanine-rich sequence repeats (in humans, the hexanucleotide motif d(TTAGGG) for example) located at the end of chromosomes, where their function is to preserve chromosome integrity. Telomeric DNA is gradually shortened in normal cells as a function of the replication cycle; this leads to cell-cycle arrest and eventually apoptosis when a critical length minimum is reached.[18] In contrast, cancer cells have evolved mechanisms to maintain telomere length, the most common of which is based on the activation of a reverse transcriptase called telomerase; this occurs in 80–90% of tumor cells.[19–21] Novel antitumor strategies are aimed at interfering with the mechanisms of telomere maintenance by targeting telomerase

[a] *Dr. C. Bazzicalupi, Prof. A. Bencini, Dr. C. Giorgi, Prof. B. Valtancoli*
Department of Chemistry "Ugo Schiff", University of Florence
Via della Lastruccia 3-13, 50019 Sesto Fiorentino, Florence (Italy)
Fax: (+39) 055-457-3364
E-mail: carla.bazzicalupi@unifi.it

[b] *Dr. M. Chioccioli, Dr. C. Bonaccini, Prof. F. Melani, Prof. P. Gratteri*
Laboratory of Molecular Modeling Cheminformatics & QSAR
Department of Pharmaceutical Sciences, University of Florence
Via Ugo Schiff 6, 50019 Sesto Fiorentino, Florence (Italy)
Fax: (+39) 055-457-3780
E-mail: paola.gratteri@unifi.it

[c] *Prof. C. Sissi, Dr. E. Porcù, Dr. C. Pivetta*
Department of Pharmaceutical Sciences, University of Padova
Via Marzolo 5, 35100 Padova, (Italy)
Fax: (+39) 049-827-5366
E-mail: claudia.sissi@unipd.it

Supporting information for this article is available on the WWW under http://dx.doi.org/10.1002/cmdc.201000332.

directly according to an enzyme recognition process, or indirectly by means of telomere-interacting agents.[22]

The human telomeres are largely double-stranded DNA sequences, but the terminal 100–200 nucleotides at the 3′ end are single stranded. This portion can easily fold into a G-quadruplex arrangement, a DNA secondary structure that consists of four guanines (G-quartet or G-tetrad) stacked in coplanar cyclic arrays associated by eight Hoogsteen hydrogen bonds. Optimal telomerase activity requires an unfolded single-stranded DNA as substrate. Therefore, ligands that selectively bind to and stabilize G-quadruplex structures may interfere with the telomerase enzymatic process.

The number of identified G-quadruplex ligands has grown rapidly over the past few years. Extensive efforts have been made to establish reliable structure–activity relationships with the aim of identifying effective and selective telomerase inhibitors. As common structural features, they generally share a large, flat, aromatic surface, and the presence of protonatable side chains.[22]

Classic dsDNA intercalators are likely to correspond to this pharmacophoric model. Indeed, several derivatives of DNA binders have also been considered as G-quadruplex binders. An interesting example is represented by acridine derivatives. Effective anticancer drugs containing this heterocyclic moiety (such as amsacrine, *m*-AMSA) are generally able to efficiently recognize DNA according to an intercalation binding mode. However, several studies have shown that by modulating the substitution pattern on this aromatic ring system, it is possible to preferentially direct such ligands toward G-quadruplex structures. In particular, a series of 3,6-disubstituted[23–25] and 3,6,9-trisubstituted acridines,[26–29] as well as some compounds characterized by a macrocyclic skeleton containing the acridine moiety[30,31] or the related quinacridine system,[32] have been reported as efficient G-quadruplex binders endowed with pharmacological anticancer properties.

On the other hand, different substitution patterns, for example at the 2,7-position, have, to date, been poorly investigated as G-quadruplex binders, because they apparently do not provide relevant G-quadruplex recognition.[33]

Herein we report the synthesis of a series of polyaza ligands featuring an acridine moiety inserted in an open-chain (L1) or macrocyclic (L2 and L3) aliphatic polyamine framework via functionalization of the 2- and 7-positions of the heteroaromatic system. These ligands enable the exploitation of the effect that a cyclic organization of the aliphatic polyamine chain has on the recognition properties for various DNA structures; thus, we decided to carry out a comprehensive study on the binding properties of L1, L2, and L3 toward telomeric G-quadruplex structures, and to compare them with their respective dsDNA binding profiles.

Results and Discussion

Ligand L1 was synthesized by reaction of 2,7-dibromomethylacridine (**1** in Scheme 1)[34] with the ditosylated amine 1-methyl-1,4-di(4-toluenesulfonyl)-1,4-diazabutane (**2**) in the presence of potassium carbonate, followed by removal of the tosyl (Ts) groups in hydrogen bromide/acetic acid in the presence of phenol as an antioxidant. Similarly, the reaction of **1** with 1,4,7,10-tetratosyl-1,4,7,10-tetraazadecane (**4**)[35] and 1,5,9,13-tetratosyl-1,5,9,13-tetraazatridecane (**5**)[36] afforded the respective tosylated macrocycles **6** and **7**, which were then deprotected in HBr/CH_3COOH/phenol, and further isolated as hydrobromide salts (L2 and L3).

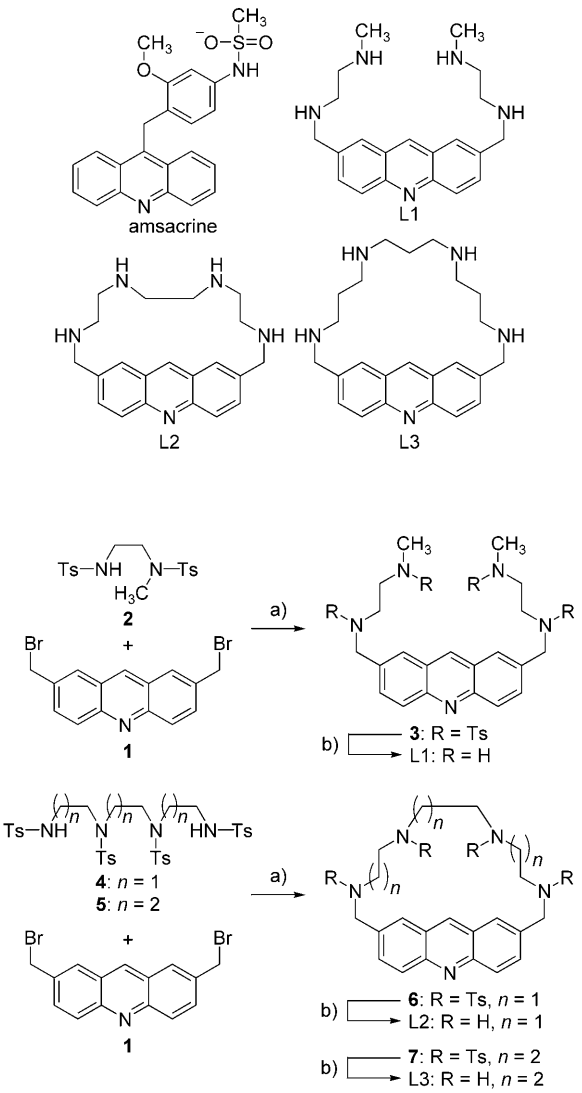

Scheme 1. Reagents and conditions: a) K_2CO_3, CH_3CN, reflux, 5 h; b) HBr, CH_3COOH, 90 °C, 24 h.

All new ligands under investigation feature one or two polyamine chains linked to the acridine moiety, and facile protonation of the amine groups occurs in aqueous solution. Ligand protonation was studied by potentiometric and ^1H NMR measurements in aqueous solution (see figures S1, S2, and a detailed description in the Supporting Information). The stepwise basicity constants ($\log K$) potentiometrically determined at 298 K, are listed in Table 1.

All ligands can bind up to five acidic protons in the 2.5–10.5 pH range investigated, effectively affording various protonated species at different alkaline to acidic pH values. In all three cases, the diprotonated form $[H_2L]^{2+}$ (L = L1, L2, or L3) is the

Table 1. Protonation constants of ligands L1–L3.[a]

Equilibrium	Log *K* L1	L2	L3
$L + H^+ = [HL]^+$	9.76(1)	10.2(1)	10.1(1)
$[HL]^+ + H^+ = [H_2L]^{2+}$	9.24(1)	8.3(1)	8.8(2)
$[H_2L]^{2+} + H^+ = [H_3L]^{3+}$	5.96(1)	5.6(1)	7.3(1)
$[H_3L]^{3+} + H^+ = [H_4L]^{4+}$	5.26(1)	3.5(2)	6.3(1)
$[H_4L]^{4+} + H^+ = [H_5L]^{5+}$	3.21(2)	3.0(1)	3.3(2)

[a] Determined potentiometrically in Me_4NCl (0.1 M) at 298 K; values in parentheses are standard deviations.

most abundant species at physiological pH. ^{1}H NMR investigations indicated that the two first protonation steps occur on the methylated nitrogen atoms in the case of L1, and on the central nitrogen atoms of the tetra-amine chain in the case of L2 and L3.

Acridine derivatives binding to dsDNA: solution studies

All derivatives were characterized spectroscopically, and their binding to ctDNA was evaluated quantitatively by monitoring the change in absorption properties of the ligands in the presence of increasing concentrations of nucleic acid. Unfortunately, under the experimental conditions used, it was not possible to quantitatively monitor the DNA binding process for L3. In fact, this ligand was very effective at inducing ctDNA precipitation at even the lowest binding ratios examined. Spectra recorded for L1 are shown as examples in Figure 1a. L2 exhibits analogous behavior. Table 2 lists the thermodynamic parameters for the binding process of L1 and L2 to calf thymus DNA, evaluated according to the McGhee and Von Hippel formalism.[37] Data for *m*-AMSA are also included for comparison.

The data in Table 2 indicate that our novel compounds have slightly higher binding affinity than *m*-AMSA. The exclusion parameter (*n*), indicating the number of DNA bases involved in ligand recognition, although slightly less in the case of L2, is close to the theoretical value of 4 required for an intercalative binding mode. This leads us to assume a similar mode of DNA interaction for *m*-AMSA and the two novel compounds.

Table 2. Thermodynamic binding parameters describing ligand–ctDNA complex formation.[a]

Ligand	K_a [10^{-5} M^{-1}]	*n* [bases]
L1	1.07 ± 0.11	5.2 ± 0.1
L2	1.55 ± 0.20	3.1 ± 0.1
m-AMSA	0.36 ± 0.03	3.2 ± 0.3

[a] Carried out in 10 mM Tris, 20 mM KCl, pH 7.5, 25 °C; K_a is the binding constant, and *n* is the exclusion number.

To clarify this point, we performed topoisomerase I unwinding assays. The assay involves incubation of supercoiled plasmid DNA with excess topoisomerase I and increasing concentrations of test compound. Topoisomerase I converts supercoiled into relaxed plasmid DNA. After removal of the drug and enzyme, re-supercoiling of the DNA occurs if the ligand had been bound by an intercalative mode.[38]

A summary of these results is shown in Figure 2. Derivatives L1 and L2 behave similarly to the reference compound *m*-AMSA, thus confirming their ability to promote DNA unwinding.[39] In contrast, L3 did not exhibit any re-supercoiling effect across the whole drug concentration range tested.

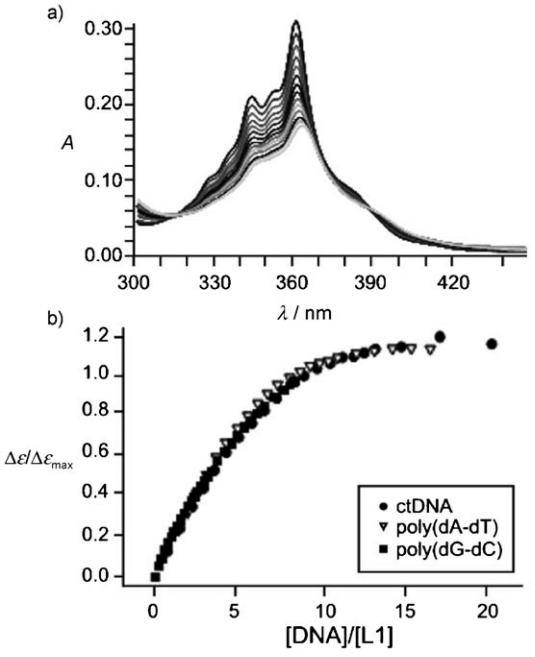

Figure 1. a) Spectral changes of L1 with increasing ctDNA concentration and b) binding isotherms for the process of L1 binding to dsDNAs of different base composition (indicated). Titrations were performed in 10 mM Tris, 20 mM KCl, pH 7.5, 25 °C.

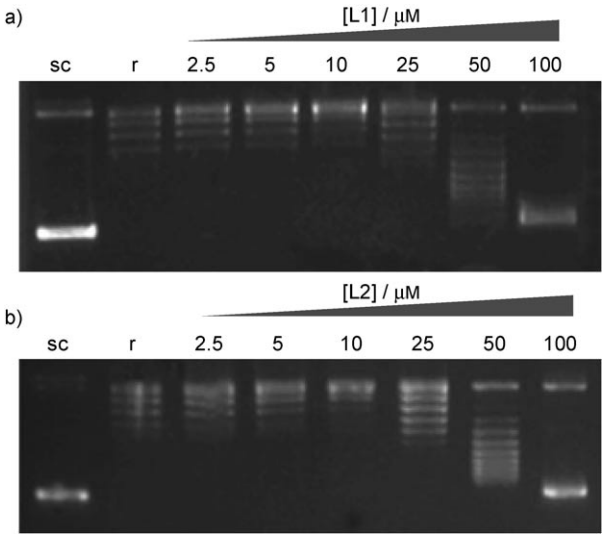

Figure 2. Topoisomerase I-mediated unwinding assays for compounds a) L1 and b) L2; sc: supercoiled DNA; r: DNA relaxed by topoisomerase I. Products were resolved on a 1% agarose gel in 1× TAE buffer.

Because the affinity of a ligand for DNA can be affected by the DNA sequence, we monitored the binding process of the three ligands to oligonucleotides of defined base composition, namely poly(dA–dT) and poly(dG–dC) (Figure 1b, showing data for L1). Binding isotherms in this figure show how the binding of L1 and L2 to the tested DNA sequences are essentially equal, and thus they confirm a lack of sequence selectivity. For comparison, the thermodynamic binding parameters for the complex formation of L1 and L2 with poly(dG–dC) are listed in Table 3.

Table 3. Thermodynamic binding parameters for complex formation of L1 and L2 with poly(dG–dC).[a]

Ligand	K_a [10^{-5} M^{-1}]	n [bases]
L1	0.89 ± 0.07	4.9 ± 0.1
L2	1.26 ± 0.18	2.8 ± 0.1

[a] Carried out in 10 mM Tris, 20 mM KCl, pH 7.5, 25 °C; K_a is the binding constant, and n is the exclusion number.

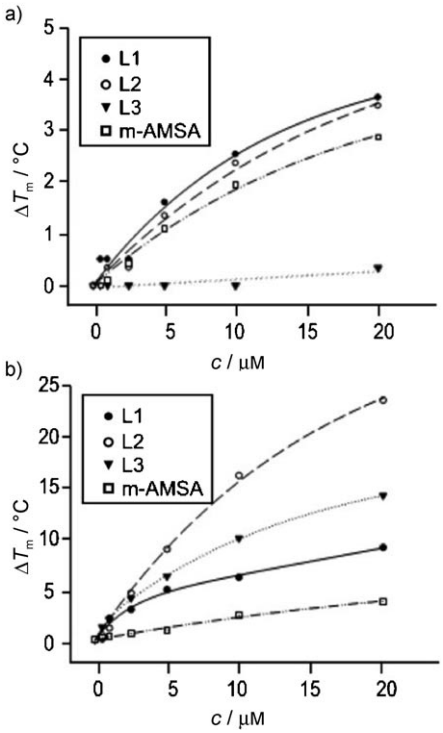

Figure 3. Variation of the melting temperature (ΔT_m) of oligonucleotides arranged into a) double-stranded or b) G-quadruplex structures upon addition of increasing concentrations of acridine derivatives in phosphate buffer containing 50 mM KCl, pH 7.4; heating rate: 0.2 °C min^{-1}.

Finally, to further evaluate the dsDNA binding properties of the novel tested ligands, we monitored the thermal stability of a dsDNA sequence in the presence of increasing drug concentrations. The target DNA was prepared by annealing two complementary oligonucleotides, one 5′-end labeled with fluorescein, and the other 3′-end labeled with a quencher (DABCYL). In the double-stranded form, the two labeling groups are in close proximity, and thus the fluorescence signal is quenched; upon dissociation (melting), the fluorescence signal is enhanced. In Figure 3a, the variation of the DNA melting temperature (T_m) induced by increasing drug concentrations is reported. Under our experimental conditions, a good correlation between unwinding data and dsDNA stabilization emerged. Indeed, L1 and L2 turned out to be effective in stabilizing dsDNA, with ΔT_m values similar to those recorded with *m*-AMSA. Conversely, L3 did not promote duplex stabilization.

Altogether, these results allowed us to draw a picture of the dsDNA binding pattern for these acridine derivatives. Although all ligands efficiently interact with DNA, the nature of the side chains plays a key role in the binding mode. Experimental results seem to suggest a preferential, non-intercalative binding mode for L3. In this case, the driving force is mainly the electrostatic interaction of the charged ligand with the nucleic acid, which promotes DNA precipitation. In contrast, L1 and L2 showed similar behavior, resembling that of *m*-AMSA, thus suggesting a more favorable balance of the π–π interactions between the acridine moiety and the base pairs, on the one hand, and the H-bond and salt bridge interactions, supported by the charged substituents, on the other.

It is well known that small macrocycles such as L2 and L3, which contain a rigid aromatic moiety in their structures, often adopt bent conformations.[40] As a consequence, one could easily propose that the insertion of the acridine moiety between DNA base pairs would be more difficult in the case of macrocycles L2 and L3 than for L1. Surprisingly, whereas no such intercalation seems to be present with L3, L2, which contains an overall shorter cyclic aliphatic chain, is still able to interact with dsDNA in a manner similar to the acyclic L1. Thus, to gain a more in-depth insight, we decided to carry out a modeling investigation.

Acridine derivatives binding to dsDNA: modeling studies

The binding mode of the diprotonated species of L1, L2, and L3 toward dsDNA was investigated by docking procedures followed by molecular dynamics (MD) simulations, with an explicit treatment of the aqueous environment.

The results shown in Figure 4 and in figure S3 (Supporting Information) largely corroborate the solution studies, as the three ligands feature different binding modes toward the poly-G–poly-C double helix. For the open-chain ligand L1, the interaction can be described as properly intercalative both in the case of the CG site, as well as for the GC site. In all situations the adduct was stabilized by additional H-bond contacts involving the terminal protonated nitrogen atoms and the carbonyl oxygen atom belonging to the cytosine and guanine units (Figure 4a), or the phosphate groups (figure S3a, Supporting Information). In fact, the planar acridine moiety of L1 can be easily lodged between the base pairs, unhindered by the pendant arms, which, on the contrary, can be set in the grooves. Moreover, the RMSD value evaluated as a function of time during the recorded MD trajectory (figure S4, Supporting

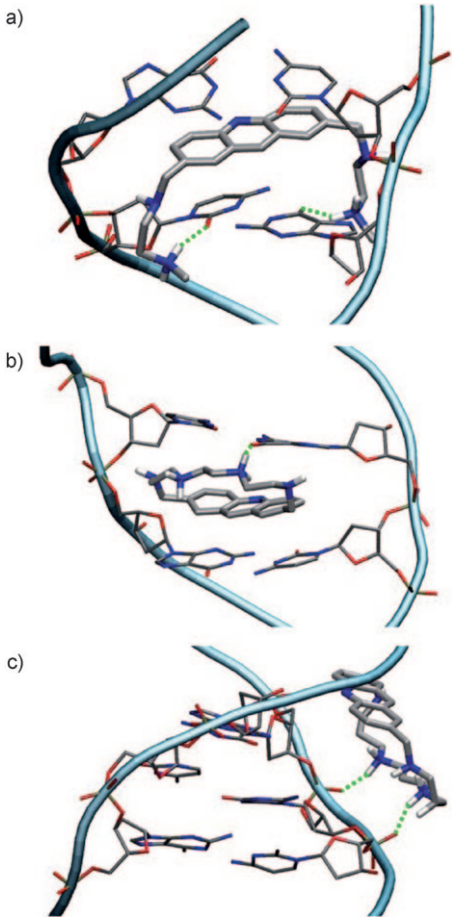

Figure 4. Results of the modeling procedures (docking and MD) for the adducts formed by diprotonated forms of a) L1, b) L2, or c) L3 and poly-G-poly-C dsDNA. Results were obtained by starting from docking in a CG intercalative binding site; hydrogen bonds are indicated by green lines.

Information) denotes that the L1–poly-G–poly-C adduct is quite stable, and it is not disrupted during the 10 ns simulation time.

On the other hand, L3, most likely hindered by the bent conformation adopted by its macrocyclic structure, seems to fail at intercalation and gives rise to groove binding, interacting mainly through hydrogen bonds between its protonated nitrogen atoms and the polyphosphate DNA backbone (Figure 4c and figure S3c, Supporting Information). After 10 ns MD simulation, the DNA double helix is almost completely rebuilt, and no trace of the CG or GC intercalative site remains.

As far as L2 is concerned, it shows an intermediate behavior between L1 and L3. In spite of its rather rigid and strained bent conformation, which is generally considered unsuitable for the stereochemical requirement of a classic DNA intercalator, modeling studies give evidence of stable conformations for the L2–DNA adduct (Figure 4b), in which the macrocycle is able to give rise to simultaneous π–π and H-bonding interactions. Indeed, L2 behaves as a multifunctional ligand toward DNA by virtue of its small size. The presence of the shorter ethylene spacers in place of propylene units featured in L3 appears to be essential for obtaining a correct match between the binding sites of L2 and the nucleobases. The relative free energies for these complexes were estimated through the molecular mechanics Poisson–Boltzmann surface area (MM-PBSA) approach. Importantly, the MM-PBSA results are in agreement with the thermodynamic parameters obtained by the solution-phase studies, showing the higher intercalative ability of L1 and L2 than that of L3 (Table 4).

Table 4. Gibbs free energy values calculated by using the MM-PBSA approach for adducts formed between ligands L1–L3 and DNA.

Ligand	ΔG [kcal mol^{-1}]		
	dsDNA[a]	dsDNA[b]	G-tetrad DNA
L1	−5.20	−5.06	−9.60
L2	−9.00	2.08	−16.54
L3	8.85	5.65	−13.47

[a] CG intercalative site. [b] GC intercalative site.

Acridine derivatives binding to G-quadruplex forming sequences: solution studies

The potential interaction of tested ligands with G-quadruplex structures was evaluated by monitoring both the stabilization and the induction of G-quadruplex structures assumed by telomeric sequences. The former were assayed by fluorescence melting experiments: in this case an oligonucleotide (HTS) was used that contains four repeats of the human telomeric sequence and which is labeled at the 5′ end with DABCYL and at the 3′ end with fluorescein. Again, upon folding into a G-quadruplex, these two labels are brought into close proximity, and fluorescence is quenched. With an increase in temperature, the DNA melts and the fluorescein signal can be detected.

As shown in Figure 3b, all our acridine derivatives can shift the G-quadruplex melting temperature to higher values. The values determined herein are lower than those reported for other G-quadruplex-selective acridine derivatives ($\Delta T_m > 30\,^{\circ}C$ was reported for BRACO-19 at 1 μM), but are relevantly higher than those observed toward dsDNA.[33] These data clearly illustrate how the efficiency of our novel ligands is modulated by the nature of the side chains. In particular, L2 appeared to be the most active in stabilizing a G-quadruplex structure, followed by L3 and L1. Notably, *m*-AMSA was confirmed to be a poor G-quadruplex binder. Thus, the similarity between L1 and L2 in the dsDNA binding properties is not conserved when the target sequence assumes a G-quadruplex structure.

To determine if this interaction reflects any ability of our new tested compounds to induce the formation of G-quadruplex structures, we performed electrophoretic mobility shift assays (EMSA), using an oligonucleotide containing only two human telomeric repeats (2GGG). This sequence can form G-quadruplex structures only by pairing two or four strands, thus leading to dimeric or tetrameric structures resolvable by polyacrylamide gel electrophoresis (Figure 5). Among the tested acridine derivatives, only L2 was able to induce the folding of 2GGG into a tetrameric G-quadruplex structure, thus confirming it as the most efficient G-quadruplex binder.

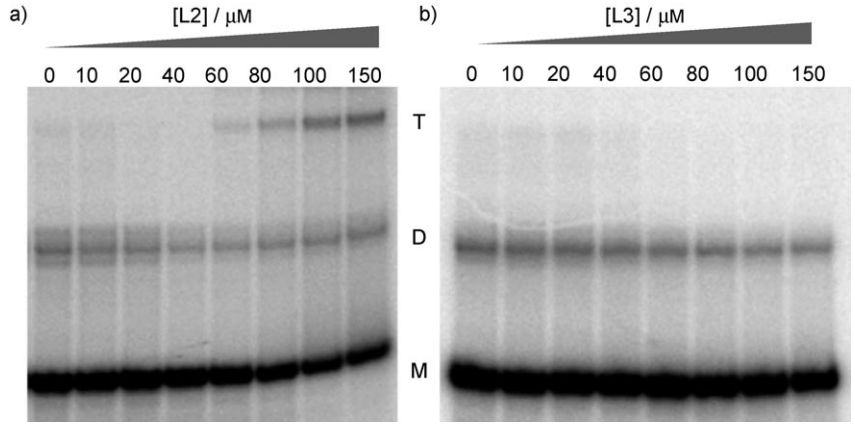

Figure 5. Effect of increasing of concentrations of a) L2 or b) L3 on the assembly of 2GGG (1 μm strand concentration) into dimeric and tetrameric G-quadruplex structures in 10 mM Tris, 1 mM EDTA, 100 mM KCl, pH 8.0, at 37 °C for 24 h. Reaction products were resolved on a 16% native polyacrylamide gel in 0.5× TBE containing 20 mM KCl; M = monomeric oligonucleotide, D = dimeric oligonucleotide, T = tetrameric G-quadruplex.

The induction of the tetrameric DNA arrangement for the 2GGG telomeric sequence correlates well with recent crystallographic data showing a related trisubstituted acridine bound to a G-quadruplex[7] with two dimeric units held together by one drug molecule stacked on the terminal G-quartets. Thus this crystallographic structure was considered a suitable model for computational studies.

Acridine derivatives binding to G-quadruplex-forming sequences: modeling studies

The orientations resulting from MD simulation carried out on selected poses of the acridine derivatives in complex with the G-quadruplex obtained from docking are shown in Figure 6. All these adducts remained quite stable during the simulation (figure S5, Supporting Information).

All ligands insert into the tetrameric form of the G-quadruplex, between the 3′-end G-tetrad belonging to one G-quadruplex dimer and the 5′-end of the other, in a manner similar to that shown by the very effective G-quadruplex ligand BRACO-19 present in the X-ray crystallographic complex structure.[7] However, the acridine moieties of L2 and L3 give rise to stronger π–π interactions with the 3′-end G-tetrad than in the case of L1, the acridine system of which shows the most significant deviation from the expected parallel position (16° between the involved planes versus 3° and 3.5° for L2 and L3, respectively). Moreover, all ligands cause, to varying degrees, a rotation of one dimeric G-quadruplex unit relative to the other. Using the BRACO-19–G-quadruplex complex as a reference, and considering the dihedral angle formed between 3′- and 5′-end G-tetrads, a 1°, 3°, and 9° twist (figure S6, Supporting Information) is observed for L2, L3, and L1, respectively.

Analysis of the L1–DNA complex shows that both π-stacking and H-bonding interactions involve only one dimer, whereas both the G-quadruplex units are simultaneously bound by L2 and L3 (Figure 6). As far as L2 and L3 are concerned, their binding modes seem similar, with both ligands interacting by π-stacking with a guanidine residue of the 5′-end G-tetrad, and by H-bonding with a phosphate group of the other dimer (Figure 6b and 6c). However, compared with L3, L2 causes a less significant disruption of the TATA tetrad, also present at the 3′- and 5′-end interface in the biological unit of the BRACO-19–DNA complex. In particular, only one adenine residue is considerably shifted from its original position, and, at the same time, the carbonyl group of a thymine residue gives rise to an additional H-bond interaction with a protonated nitrogen of the ligand, thus exerting a significant role in the stabilization of the adduct (Figure 6b). However, in the case

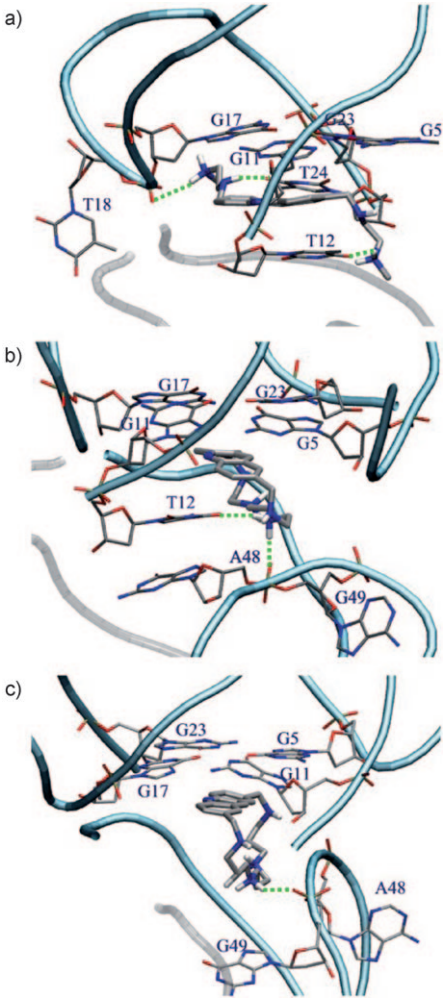

Figure 6. Results of MD simulations of the adducts formed by the diprotonated species a) L1, b) L2, and c) L3 with the G-quadruplex structure formed by the 2GGG oligonucleotide. Hydrogen bonds are indicated by green lines; interacting and non-interacting DNA monomers (tube representation) are colored in light blue and gray, respectively.

of the L3 complex, both the aforementioned adenine and thymine residues are in a different position, and no additional H-bond contacts are established.

Altogether, the observations derived from the modeling procedures support the quite surprising results obtained from the solution studies, which show evidence that the bent conformations of L2 and L3 do not prevent G-quadruplex recognition. The binding free energy values obtained by the MM-PBSA calculations indicate that binding affinity decreases in the order L2 > L3 > L1 (Table 4), in agreement with the reported solution studies.

Enzymatic and cellular activity

From the results discussed above, L2 turns out to be a potential telomerase inhibitor. Therefore, we decided to determine whether L2 is able to efficiently interfere with the enzyme-mediated elongation process of a proper template. Indeed, we observed that L2 can efficiently inhibit telomerase activity with an IC_{50} value of 1.7 μM, well below the drug concentration required to interfere with the Taq polymerase amplification process (10 μM; figure S7, Supporting Information). For comparison, L1 was tested in the same way, and it was confirmed to be unable to decrease telomerase activity.

Finally, the toxicity of tested compounds was evaluated with the HeLa cancer cell line, and the results are summarized in Table 5. Our data show that after drug exposure for 72 h, all novel derivatives are less cytotoxic than *m*-AMSA. The most cytotoxic compound is derivative L3, with an IC_{50} value of 32 μM, whereas for L2 and L4, IC_{50} values are > 100 μM.

Table 5. IC_{50} values for all tested compounds obtained in HeLa cells.

Compd	IC_{50} [μM]
m-AMSA	2.0 ± 0.4
L1	> 100
L2	> 100
L3	32 ± 6.2

This result is an interesting starting point. Indeed, a canonical telomerase inhibitor can be devoid of any toxic effect after such short time exposures. Thus the properties associated with the G-quadruplex interaction profile of L2, as revealed through our work, indicate this compound to be a suitable lead candidate worthy of further optimization.

Conclusions

The new 2,7-substituted acridine derivatives L1, L2, and L3 show an unusual trend in their binding patterns toward canonical double-helical DNA and non-canonical G-quadruplex structures. The DNA recognition profile of L1 is in line with the expectation, as it parallels the behavior shown by *m*-AMSA: it binds to dsDNA through a pure intercalative process and poorly recognizes G-quadruplex structures. Ligand L2 features a small macrocyclic framework which is generally expected to adopt a rather bent and rigid conformation, usually not prone to intercalative interactions with DNA. However, in spite of this, L2 binds to dsDNA almost as well as the open-chain ligand L1, and it shows the best performance toward a G-quadruplex. Distinctly, ligand L3, characterized by the same cyclic structure of L2, but with longer and more flexible propylene spacers, should, in principle, be able to adopt a planar conformation more readily. Nevertheless, it is unable to intercalate into dsDNA, nor can it induce G-quadruplex structures.

As pointed out by the molecular modeling studies, the better performance of L2 relative to that of L3 and the open-chain ligand L1 can be attributed entirely to its particular conformation and dimensions, which establish an optimal match with both dsDNA and the tetrameric G-quadruplex structure.

The distinct DNA binding modes characterized for our novel ligands could explain their effect on telomerase, with L2 being a good inhibitor of this enzyme, a property that is coupled with favorably low short-term cytotoxicity. These results indicate how important it is to set up simultaneous combinations of interactions of various kinds between DNA and ligand in order to reach an optimal binding efficiency, thus effectively opening new possibilities for the design of novel selective DNA binders.

Experimental Section

Materials

The human telomeric sequence HTS 5′-[DABCYL]-AGG-GTT-AGG-GTT-AGG-GTT-AGG-GT-[FAM]-3′ was synthesized and purified by ATDBIO (Southampton, UK). Oligonucleotides 2GGG (5′-TAC-AGA-TAG-TTA-GGG-TTA-GGG-TTA-3′), 1GGG (5′-TAC-AGA-TAG-TTA-GGG-TTA-GAC-TTA-3′), poly(dA–dT)$_{25}$, poly(dG–dC)$_{25}$, QMup (5′-[FAM]-GTG-AGA-TAC-CGA-CAG-AAG-3′), QMdown (5′-CTT-CTG-TCG-GTA-TCT-CAC-[DABCYL]-3′), TS (5′-AAT-CCG-TCG-AGC-AGA-GTT-3′), ACX (5′-GTG-CCC-TTA-CCC-TTA-CCC-TTA-CCC-TAA-3′), Tup (5′-TGA-GGA-TCC-GCC-TGG-ACA-GCA-TGG-3′), and Tdown (5′-GTC-GAA-TTC-TCG-GCG-AGA-AGC-AGG-3′) were provided by Eurogentec (Belgium). QMup and QMdown were mixed at equimolar concentrations, heated at 95 °C for 5 min, and then cooled to room temperature overnight before use. Calf thymus DNA (ctDNA) and plasmid pBR322 were purchased from Sigma–Aldrich (USA) and Fermentas, respectively, and used with no further purification. Reagents and solvents for synthesis were purchased from Aldrich and used without further purification.

Ligand synthesis

Ligands L1, L2, and L3 were synthesized by reaction of 2,7-dibromomethylacridine (**1**, Scheme 1)[34] with 1-methyl-1,4-ditosyl-1,4-diazabutane (**2**), 1,4,7,10-tetratosyl-1,4,7,10-tetraazadecane (**4**),[35] and 1,5,9,13-tetratosyl-1,5,9,13-tetraazatridecane (**5**).[36] The resulting tosylated products **3**, **6**, and **7** were deprotected in a mixture of HBr/CH_3COOH.

Bis[*N*,*N*′-bistosyl-2-methylaminoethylaminomethyl]-(2,7)-acridine (3): A suspension of **1** (1.91 g, 5.233 mmol) in dry CH_3CN (170 mL) was added dropwise over a period of 4 h to a and vigorously stirred suspension of **2** (5.21 g, 13.6 mmol) and K_2CO_3 (13.6 g,

0.1 mol) in dry CH_3CN (80 mL) at reflux. After the addition was completed, the solution was held at reflux for an additional 5 h. The resulting suspension was filtered, and the solution was evaporated under vacuum to give a crude oil, which was purified by column chromatography on neutral alumina (activity II/III, CH_2Cl_2/EtOAc, 8:1 *v/v* as eluent). The eluted fractions were collected and evaporated to dryness to afford **3** as a white solid. Yield: 1.98 g (2.04 mmol, 39%); elemental analysis: calcd (%) for $C_{49}H_{53}N_5S_4O_8$: C 60.79, H 5.52, N 7.23, found: C 61.1, H 5.4, N 7.3.

Bis(2-methylaminoethylaminomethyl)-(2,7)-acridine pentahydrobromide (L1·5 HBr·H_2O): Compound **3** (0.97 g, 1 mmol) and phenol (10.5 g, 0.112 mol) were dissolved in a mixture of HBr/CH_3COOH (33%, 100 mL). The reaction was stirred at 90 °C for 24 h until a precipitate was formed. The solid was filtered out and washed several times with CH_2Cl_2. The pentahydrobromide salt was recrystallized from EtOH/H_2O (3:1) to yield 0.41 g (0.525 mmol, 52.5%). Elemental analysis: calcd (%) for $C_{21}H_{29}N_5$·5 HBr·H_2O: C 32.59, N 9.05, H 4.69, found: C 32.6, N 9.1, H 4.7; ^{1}H NMR (D_2O, pH 2.50): $\delta = 9.60$ (s, 1H), 8.50 (s, 2H), 8.38 (d, 2H), 8.18 (d, 2H) 4.65 (s, 4H), 3.64 (m, 4H), 3.53 (m, 4H), 2.84 ppm (s, 6H); ^{13}C NMR (D_2O, pH 2.50): $\delta =$ 150.6, 139.8, 138.5, 131.9, 130.3, 125.9, 120.65, 50.6, 44.3, 42.9, 33.3 ppm.

2,4,7,10-Tetratosyl-2,4,7,10-tetraaza[12]-(2,7)-acridinophane (6): A suspension of **1** (1.40 g, 3.83 mmol) in dry CH_3CN (140 mL) was added dropwise over a period of 4 h to a vigorously stirred suspension of **4** (3.5 g, 4.59 mmol) and K_2CO_3 (9.82 g, 71.0 mmol) in dry CH_3CN (70 mL) at reflux. After the addition was completed, the solution was held at reflux for an additional 5 h. The resulting suspension was filtered, and the solution was evaporated under vacuum to give a crude oil, which was purified by column chromatography on neutral alumina (activity II/III, CH_2Cl_2/EtOAc, 8:1 *v/v* as eluent). The eluted fractions were collected and evaporated to dryness to afford **6** as a white solid. Yield: 1.55 g (1.60 mmol 41.8%); elemental analysis: calcd (%) for $C_{49}H_{51}N_5S_4O_8$: C 60.91, H 5.32, N 7.25, found: C, 60.8; H, 5.3; N, 7.2.

2,4,7,10-Tetraaza[12]-cyclo(2,7)-acridinophane pentahydrobromide (L2·5 HBr): Compound **6** (1.00 g, 1 mmol) and phenol (10.5 g, 0.112 mol) were dissolved in a mixture of HBr/CH_3COOH (33%, 100 mL). The reaction was stirred at 90 °C for 24 h until a precipitate was formed. The solid was filtered out and washed several times with CH_2Cl_2. The pentahydrobromide salt was recrystallized from EtOH/H_2O (3:1) to yield 0.51 g (0.68 mmol, 68%). Elemental analysis: calcd (%) for $C_{21}H_{27}N_5$·5 HBr: C 33.45, N 9.29, H 4.28, found: C 33.3, N 9.2, H 4.3; ^{1}H NMR (D_2O, pH 4.10): $\delta = 9.89$ (s, 1H), 8.62 (s, 2H), 8.36 (d, 2H), 8.24 (d, 2H) 4.61 (s, 4H), 3.51 (m, 4H), 3.41 (m, 4H), 3.29 ppm (s, 4H); ^{13}C NMR (D_2O, pH 4.10): $\delta = 149.30$, 141.32, 138.29, 132.66, 131.05, 126.35, 122.41, 49.66, 44.56, 44.40, 42.63 ppm.

2,6,10,14-Tetratosyl-2,6,10,14-tetraaza[15]-(2,7)-acridinophane (7): This compound was synthesized in dry CH_3CN from **1** (1.00 g, 2.74 mmol), **5** (2.64 g, 3.28 mmol), and K_2CO_3 (7.03 g, 50.9 mmol) by following the procedure reported above for **6**. Yield: 1.40 g (1.39 mmol, 51%); elemental analysis: calcd (%) for $C_{52}H_{57}N_5S_4O_8$: C 61.94, H 5.70, N 6.95, found: C 61.8, H 5.6, N 6.8.

2,6,10,14-Tetraaza[15]-cyclo(2,7)-acridinophane pentahydrobromide (L3·5 HBr·H_2O): This **c**ompound was synthesized in a mixture of HBr/CH_3COOH (33%) from **7** (1.00 g, 1 mmol) in the presence phenol (10.5 g, 0.112 mol) by following the procedure described for **L2**. Yield: 0.61 g (0.75 mmol, 75%); elemental analysis: calcd (%) for $C_{24}H_{33}N_5$·5 HBr·H_2O: C 35.41, N 8.60, H 4.95, found: C 35.5, N 8.6, H 5.0; ^{1}H NMR (D_2O, pH 4.26): $\delta = 9.09$ (s, 1H), 8.31 (s, 2H), 8.16 (d, 2H), 7.93 (d, 2H) 4.59 (s, 4H), 3.06 (m, 4H), 2.71 (m, 4H), 2.23 (m, 4H), 1.66 (m, 4H), 1.44 ppm (m, 2H); ^{13}C NMR (D_2O, pH 4.26): $\delta = 149.31$, 141.33, 138.39, 132.76, 130.04, 126.44, 122.42, 49.69, 44.64, 44.40, 42.66, 22.23, 21.94 ppm.

Potentiometric measurements. Potentiometric titrations ($-\log[H^+]$) were carried out with 0.1 M $N(CH_3)_4Cl$ ($pK_w = 13.83$) at 25.0 ± 0.1 °C by using equipment and procedures previously described.[41] The computer program HYPERQUAD[42] was used to calculate the protonation constants of the ligands from emf data. Distribution diagrams were calculated by using the Hyss program.[43]

NMR spectroscopic measurements. ^{1}H (300.07 MHz) and ^{13}C (75.46 MHz) NMR spectra were recorded at 298 K in $CDCl_3$ and D_2O solutions at various pH values on a Varian Gemini 300 spectrometer. Small amounts of 0.01 M NaOD and DCl were added to the solutions to adjust the pD. The pH was calculated from the measured pD values by using the relationship: pH = pD − 0.40.[44]

DNA binding studies. Ligand–DNA spectroscopic titrations were performed at 25 °C in 10 mM Tris, 20 mM KCl, pH 7.5 with a PerkinElmer Lambda 20 apparatus equipped with a Haake F3-C thermostat. Binding was monitored by recording the signal in the ligand absorption range after the addition of scalar amounts of DNA to a freshly prepared drug solution. For each drug/DNA ratio, the fraction of bound ligand was calculated [$\nu = (\varepsilon - \varepsilon_0)/(\varepsilon_\infty - \varepsilon_0)$, for which ε_0 and ε_∞ are the extinction coefficients of the free and DNA-bound ligand, respectively]. Data were evaluated according to the equation derived by McGhee and Von Hippel.[37]

Topoisomerase I DNA unwinding assay. Supercoiled pBR322 plasmid DNA (0.15 μg) was incubated with 1 U topoisomerase I (Invitrogen) and increasing concentrations of tested compounds for 24 h at 37 °C. Reactions were terminated by two extractions with one volume of phenol/$CHCl_3$/isoamyl alcohol (25:24:1). Samples were loaded on an agarose gel (1%) and run at 40 V for 3 h. Gels were stained with ethidium bromide and photographed.

Fluorescence melting studies. The melting temperature of fluorescein-labeled DNAs in the presence or absence of ligands was determined by fluorescence melting experiments performed in a Roche LightCycler, using an excitation source at λ 488 nm, and reading the fluorescence emission at λ 520 nm. Melting experiments were performed in a total volume of 20 μL containing 0.25 μM DNA and variable concentrations of tested derivatives in LiP buffer (10 mM LiOH, 50 mM KCl, pH 7.4 with H_3PO_4). Reaction mixtures were first denatured by heating at 95 °C for 5 min, and then cooled to 30 °C at a rate of 0.5 °C min^{-1}. The temperature was then slowly increased (0.2 °C min^{-1}) up to 90 °C and again lowered at the same rate to 30 °C. Recordings were taken during both the melting and annealing processes to check for hysteresis. T_m values were determined from the first derivatives of the melting profiles using the Roche LightCycler software. Each curve was repeated at least three times, and errors were ± 0.4 °C.

Electrophoretic mobility shift assay. Single-stranded oligomer 2GGG was 5′-end labeled with ^{32}P. DNA was allowed to fold overnight, and then increasing ligand concentrations in 10 mM Tris-HCl, 1 mM EDTA, 50 mM KCl, pH 8.0 were added. Reaction mixtures were incubated at 25 °C for 30 min and then loaded on native (non-denaturing) 16% polyacrylamide gels. Electrophoresis proceeded for 3 h in 0.5× TBE supplemented with 20 mM KCl. Gels were dried, and the resolved bands were visualized and quantified on a PhosphorImager (Amersham).

Taq polymerase assay. To meet proper working conditions, compounds were assayed against Taq polymerase activity by using

pBR322 (2.5 ng) as a DNA template and appropriate primer sequences Tup and Tdown (0.5 μM) to amplify the 906–1064 sequence of the plasmid by PCR. The reaction was carried out in an Eppendorf thermocycler performing 25 cycles of: 30 s at 94 °C, 30 s at 65 °C, and 30 s at 72 °C. The reaction products were resolved on a 2% agarose gel in TBE (89 mM Tris base, 89 mM boric acid, 2 mM Na_2EDTA) and stained by ethidium bromide.

Telomerase activity (TRAP) assay. An aliquot of 5×10^6 HeLa cells in exponential growth phase was pelleted and lysed for 30 min on ice using 100 μL 0.5% CHAPS, 1 mM EGTA, 25% 2-mercaptoethanol, 1.74% PMSF, and glycerol (10% *w/v*). The lysate was centrifuged at 13000 rpm (21500×*g*) for 30 min at 4 °C, and the supernatant was collected, stored at −80 °C, and used as a telomerase source. Telomerase activity was assayed by using a modified telomere repeat amplification protocol (TRAP) assay.[45] Briefly, a proper substrate TS (100 ng) was elongated by telomerase by incubation of the reaction mixture with 1 μg protein extract at 37 °C for 30 min in the presence or absence of increasing drug concentrations. Product amplification was then performed by the addition of 100 ng return primer ACX and 2 U Taq polymerase and PCR amplification (33 cycles of: 30 s at 92 °C, 30 s at 58 °C, and 45 s at 72 °C). The reaction products were resolved by a 10% polyacrylamide gel (19:1) in TBE and visualized after staining with Sybr Green I. Telomerase inhibition values are expressed as percent of telomerase inhibition relative to control (no drug) lanes.

Cell toxicity assay. The HeLa (human epithelial) cell line was maintained in DMEM supplemented with 10% heat-inactivated fetal calf serum, 50 U mL^{-1} penicillin G, and 50 μg mL^{-1} streptomycin at 37 °C under a humidified atmosphere and 5% CO_2. For the MTT assay, cells were plated in 96-well plates at 10000 cells per well, and cultured overnight. Afterward, compounds were added in triplicate, and plates were incubated in the presence of the drug for 72 h. At the end of this period, MTT [3-(4,5-dimethylthiazol-2-yl)-2,5-diphenyltetrazolium bromide, a yellow tetrazole] was added to a final concentration of 0.8 mg mL^{-1}, and incubation was continued for an additional 2 h. After removal of the medium, DMSO was added (150 μL per well). Soluble formazan salts formed by living cells were homogenized by manual pipetting, and the absorbance at λ 540 nm was read. Results were analyzed as sigmoidal dose–response curves.

Computational methods. The binding capacity of H_2L1^{2+}, H_2L2^{2+}, and H_2L3^{2+} toward the telomeric G-quadruplex structure of sequence d(TAG-GGT-TAG-GGT) and toward double-helical DNA oligonucleotides (10-mers) of base composition poly(dG–dC) was investigated. Ligand molecules and dsDNA containing CG or GC intercalative binding sites were built by the Build module of Maestro v. 8.5.[46] Starting coordinates for the tetrameric G-quadruplex were obtained from the biological unit of the BRACO-19–d(TAG-GGT-TAG-GGT) complex X-ray crystal structure (PDB ID: 3CE5).[7]

Docking calculations were performed using Glide[47] with the DNA structures kept fixed in their original conformation throughout the docking procedures. Selected poses of the ligand–target (both dsDNA and G-quadruplex) complexes were submitted to MD simulation for 10 ns in explicit solvent, and the RMSD values of the complexes were monitored as a function of simulation time.

The atomic electrostatic charges of the ligands were calculated by means of the RESP procedure,[48] that is, fitting them to an electrostatic potential calculated at the HF/6-31G* level of theory using Gaussian 09 software.[49] General Amber force field (GAFF) parameters were then assigned to the ligands by the *antechamber* module implemented in AMBER9 suite.[50] Each complex was immersed in a truncated octahedral box, the edges of which were located 10 Å from the closest atom of the DNA fragments, and which contains ~4700 water molecules for the poly(dG–dC) dsDNA oligonucleotides, and ~5800 water molecules for the G-quadruplex complexes. To maintain neutrality in the system, 16 and 38 K^+ counterions were added to the solvent bulk of the dsDNA–water complexes and to the solvent bulk of the G-quadruplex–water complexes, respectively. In the case of the G-quadruplex structure, according to X-ray data,[7] 4 K^+ ions were placed along the axis within the central core of the complex, midway between each G-tetrad. Before starting the MD simulations, an energy minimization of the complexes was performed by setting a convergence criterion on a gradient of 0.01 kcal mol^{-1} Å^{-1}. Water shells and counterions were then equilibrated for 40 ps at 300 K, after which 10 ns of MD simulation in an isothermal-isobaric ensemble was performed without any restraint on each complex. The ff03 version of the AMBER force field was used for the DNA fragments and the counterions,[51] whereas the TIP3P model[52] was employed to explicitly represent water molecules. In the production runs, the ligand–DNA fragment systems were simulated in periodic boundary conditions. The van der Waals and short-range electrostatic interactions were estimated within a 10 Å cutoff, whereas the long-range electrostatic interactions were assessed by using the particle mesh Ewald method,[53] with 1 Å charge grid spacing interpolated by fourth-order *B*-spline, and by setting the direct sum tolerance to 10^{-5}. Bonds involving hydrogen atoms were constrained by using the SHAKE algorithm[54] with a relative geometric tolerance for coordinate resetting of 0.00001 Å. Berendsen's coupling algorithms[55] were used to maintain constant temperature and pressure with the same scaling factor for both solvent and solutes, and with the time constant for heat-bath coupling maintained at 1.5 ps. The pressure for the isothermal-isobaric ensemble was regulated by using a pressure relaxation time of 1 ps in the Berendsen's algorithm. The simulations of the solvated complexes were performed using a constant pressure of 1 atm and a constant temperature of 300 K. A time step of 2 fs was used in the simulations, which were carried out with the AMBER9 program suite.[50]

MM-PBSA calculations. Free energies were calculated by using the MM-PBSA method. The electrostatic contribution to the solvation free energy was calculated with the nonlinear Poisson–Boltzmann method as implemented in the adaptive Poisson–Boltzmann solver (APBS)[56] program through the AMBER/iAPBS interface. The hydrophobic contribution to the solvation free energy was determined with terms dependent on solvent-accessible surface area. In these calculations, we used a solvent probe radius of 1.4 Å to define the dielectric boundary, a physiological salt concentration of 0.154 M to calculate the effect of salt on the free energies, and dielectric constants of 1.0 and 80.0, respectively, for the solute and surrounding solvent. Atomic charges for DNA fragments and ligands are the same as those employed in the MD simulations. For atomic radii, we applied the PARSE[57] parameter set. In the case of the G-quadruplex structures, the cations (K^+) present within the negatively charged central channel were also explicitly included in the calculation. The K^+ ion radius was kept at 2.025 Å, based on a previous study.[58] Free energies were estimated by collecting snapshots every 40 ps during the last 4 ns of the MD simulations.

The entropic contribution was estimated with the normal mode analysis (Nmode[59] module of AMBER9 suite); the snapshots were minimized in the gas phase for a maximum of 1×10^5 cycles to give an energy gradient of 1×10^{-4} kcal mol^{-1} Å^{-1}. Because of the extensive computational requirement, the normal mode analyses were performed by considering snapshots collected every 200 ps

during the last 4 ns of the MD simulations. Molecular graphics were produced with Visual Molecular Dynamics (VMD)[60] and Mercury.[61]

Acknowledgements

We are grateful to MIUR and Ministero dell'Istruzione, dell'Università e della Ricerca, (PRIN 2007) for financial support.

Keywords: acridine derivatives · DNA · G-quadruplexes · MM-PBSA · molecular dynamics

[1] S. Neidle, *Prog. Med. Chem.* **1979**, *16*, 151 – 221.
[2] H. M. Berman, P. R. Yuong, *Annu. Rev. Biophys. Bioeng.* **1981**, *10*, 87 – 114.
[3] W. P. Wilson, R. L. Jones, *Adv. Pharmcol. Chemother.* **1981**, *18*, 177 – 222.
[4] S. Haider, G. N. Parkinson, M. A. Read, S. Neidle in *DNA and RNA Binders. From Small Molecules to Drugs* (Eds.: M. Demeunynck, C. Bailly, W. D. Wilson), Wiley-VCH, Weinheim, **2003**, pp. 337 – 359.
[5] J. E. Reed, S. Neidle, R. Vilar, *Chem. Commun.* **2007**, 4366 – 4368.
[6] G. N. Parkinson, R. Ghosh, S. Neidle, *Biochemistry* **2007**, *46*, 2390 – 2397.
[7] N. H. Campbell, G. N. Parkinson, A. P. Reszka, S. Neidle, *J. Am. Chem. Soc.* **2008**, *130*, 6722 – 6724.
[8] J. Dai, M. Carver, D. Yang, *Biochimie* **2008**, *90*, 1172 – 1183, and references therein.
[9] J. L. Mergny, C. Helene, *Nat. Med.* **1998**, *4*, 1366 – 1367.
[10] D. Y. Sun, L. H. Hurley in *Methods in Enzymology, Drug–Nucleic Acid Interactions, Vol. 340* (Eds.: J. B. Chaires, M. J. Waring), Academic Press Inc., San Diego, **2001**, pp. 573 – 592.
[11] L. H. Hurley, *Nat. Rev. Cancer* **2002**, *2*, 188 – 200.
[12] S. Neidle, G. N. Parkinson, *Nat. Rev. Drug Discovery* **2002**, *1*, 383 – 393.
[13] A. G. Bodnar, M. Ouellette, M. Frolkis, S. E. Holt, C. P. Chiu, G. B. Morin, C. B. Harley, J. W. Shay, S. Lichtsteiner, W. E. Wright, *Science* **1998**, *279*, 349 – 352.
[14] C. B. Harley, *Mutat. Res.* **1991**, *256*, 271 – 282.
[15] J. A. Hackett, D. M. Feldser, C. W. Greider, *Cell* **2001**, *106*, 275 – 286.
[16] H. Sun, J. K. Karow, I. D. Hickson, N. Maizels, *J. Biol. Chem.* **1998**, *273*, 27587 – 27592.
[17] H. Sun, R. J. Bennett, N. Maizels, *Nucleic Acids Res.* **1999**, *27*, 1978 – 1984.
[18] C. B. Harley, A. B. Futcher, C. W. Greider, *Nature* **1990**, *345*, 458 – 460.
[19] C. W. Greider, E. H. Blackburn, *Cell* **1985**, *43*, 405 – 413.
[20] G. B. Morin, *Cell* **1989**, *59*, 521 – 529.
[21] N. W. Kim, M. A. Piatyszek, K. R. Prowse, C. B. Harley, M. D. West, P. L. C. Ho, G. M. Coviello, W. E. Wright, S. L. Weinrich, J. W. Shay, *Science* **1994**, *266*, 2011 – 2015.
[22] A. De Cian, L. Lacroix, C. Douarre, N. Temime-Smaali, C. Trentesaux, J.-F. Riou, J.-L. Mergny, *Biochimie* **2008**, *90*, 131 – 155.
[23] R. J. Harrison, S. M. Gowan, L. R. Kelland, S. Neidle, *Bioorg. Med. Chem. Lett.* **1999**, *9*, 2463 – 2468.
[24] M. A. Read, A. A. Wood, J. R. Harrison, S. M. Gowan, L. R. Kelland, H. S. Dosanjh, S. Neidle, *J. Med. Chem.* **1999**, *42*, 4538 – 4546.
[25] C. M. Schultes, W. Guyen, J. Cuesta, S. Neidle, *Bioorg. Med. Chem. Lett.* **2004**, *14*, 4347 – 4351.
[26] M. Read, R. J. Harrison, B. Romagnoli, F. A. Tanious, S. H. Gowan, A. P. Reszka, W. D. Wilson, L. R. Kelland, S. Neidle, *Proc. Natl. Acad. Sci. USA* **2001**, *98*, 4844 – 4849.
[27] S.M Gowan, J. R. Harrison, L. Patterson, M. Valenti, M. A. Read, S. Neidle, L. R. Kelland, *Mol. Pharmacol.* **2002**, *61*, 1154 – 1162.
[28] R. J. Harrison, J. Cuesta, G. Chessari, M. A. Read, S. K. Basra, A. P. Reszka, J. Morrell, S. M. Gowan, C. M. Incles, F. A. Tanious, W. D. Wilson, L. R. Kelland, S. Neidle, *J. Med. Chem.* **2003**, *46*, 4463 – 4476.
[29] C. Martins, M. Gunaratnam, J. Stuart, V. Makwana, O. Greciano, A. P. Reska, L. R. Kelland, S. Neidle, *Bioorg. Med. Chem. Lett.* **2007**, *17*, 2293 – 2298.
[30] P. Alberti, J. Ren, M. P. Teulade-Fichou, L. Guittat, J. F. Riou, J. B. Chaires, C. Hélène, J. P. Vigneron, J. M. Lehn, J. L. Mergny, *J. Biomol. Struct. Dyn.* **2001**, *19*, 505 – 513.
[31] M. Kaiser, A De Cian, M. Sainlos, C. Renner, J. L. Mergny, M. P. Teulade-Fichou, *Org. Biomol. Chem.* **2006**, *4*, 1049 – 1057.
[32] C. Hounsou, L. Guittat, D. Monchaud, M. Jourdan, N. Saettel, J. L. Mergny, M. P. Teulade-Fichou, *ChemMedChem* **2007**, *2*, 655 – 666.
[33] R J. Harrison, A. P. Reszka, S. M. Haider, B. Romagnoli, J. Morrell, M. A. Read, S. M. Gowan, C. M. Incles, L. R. Kelland, S. Neidle, *Bioorg. Med. Chem. Lett.* **2004**, *14*, 5845 – 5849.
[34] S. Bartoli, C. Bazzicalupi, S. Biagini, L. Borsari, A. Bencini, E. Faggi, C. Giorgi, C. Sangregorio, B. Valtancoli, *Dalton Trans.* **2009**, 1223 – 1230.
[35] A. Bencini, A. Bianchi, E. Garcia-Espana, M. Giusti, M. Micheloni, P. Paoletti, *Inorg. Chem.* **1987**, *26*, 681 – 684.
[36] C. Bazzicalupi, A. Beconcini, A. Bencini, V. Fusi, C. Giorgi, A. Masotti, B. Valtancoli, *J. Chem. Soc. Perkin Trans. 2* **1999**, 1675 – 1682.
[37] J. D. McGhee, P. H. Von Hippel, *J. Mol. Biol.* **1974**, *86*, 469 – 489.
[38] S. M. Zeman, D. M. Crothers, *Methods Enzymol.* **2001**, *340*, 51 – 68.
[39] Y. Pommier, J. M. Covey, D. Kerrigan, J. Markovits, R. Pham, *Nucleic Acids Res.* **1987**, *15*, 6713 – 6731.
[40] For some recent examples see Ref. [34] and: a) C. Bazzicalupi, A. Bencini, S. Biagini, E. Faggi, S. Meini, C. Giorgi, A. Spepi, B. Valtancoli, *J. Org. Chem.* **2009**, *74*, 7349 – 7363; b) M. C. Aragoni, M. Arca, A. Bencini, S. Biagini, A. J. Blake, C. Caltagirone, F. Demartin, G. De Filippo, F. A. Devillanova, A. Garau, K. Gloe, F. Isaia, V. Lippolis, B. Valtancoli, M. Wenzel, *Inorg. Chem.* **2008**, *47*, 8391 – 4303; c) C. Cruz, R. Delgado, M. G. B. Drew, V. Felix, *J. Org. Chem.* **2007**, *72*, 4023 – 4034; d) C. Bazzicalupi, A. Bencini, A. Bianchi, L. Borsari, A. Danesi, C. Giorgi, C. Lodeiro, P. Mariani, F. Pina, S. Santarelli, A. Tamayo, B. Valtancoli, *Dalton Trans.* **2006**, 4000 – 4010.
[41] C. Lodeiro, A. J. Parola, F. Pina, C. Bazzicalupi, A Bencini, A Bianchi, C. Giorgi, A. Masotti, B. Valtancoli, *Inorg. Chem.* **2001**, *40*, 2968 – 2975
[42] P. Gans, A. Sabatini, A Vacca, *Talanta* **1996**, *43*, 1739 – 1753.
[43] L. Alderighi, P. Gans, A. Ienco, D. Peters, A. Sabatini, A. Vacca, *Coord. Chem. Rev.* **1999**, *184*, 311 – 318.
[44] A. K. Covington, M. Paabo, R. A. Robinson, R. G. Bates, *Anal. Chem.* **1968**, *40*, 700 – 706.
[45] N. W. Kim, F. Wu, *Nucleic Acids Res.* **1997**, *25*, 2595 – 2597.
[46] Maestro v. 8.5, Schrödinger, LLC, New York, NY (USA), 2007.
[47] Glide, v. 4.5, Schrödinger, LLC, New York, NY (USA), 2007.
[48] C. I. Bayly, P. Cieplak, W. D. Cornell, P. A. Kollman, *J. Phys. Chem.* **1993**, *97*, 10269 – 10280.
[49] Gaussian 09 (Revision A.01), M. J. Frisch, G. W. Trucks, H. B. Schlegel, G. E. Scuseria, M. A. Robb, J. R. Cheeseman, G. Scalmani, V. Barone, B. Mennucci, G. A. Petersson, H. Nakatsuji, M. Caricato, X. Li, H. P. Hratchian, A. F. Izmaylov, J. Bloino, G. Zheng, J. L. Sonnenberg, M. Hada, M. Ehara, K. Toyota, R. Fukuda, J. Hasegawa, M. Ishida, T. Nakajima, Y. Honda, O. Kitao, H. Nakai, T. Vreven, J. A., Jr., Montgomery, J. E. Peralta, F. Ogliaro, M. Bearpark, J. J. Heyd, E. Brothers, K. N. Kudin, V. N. Staroverov, R. Kobayashi, J. Normand, K. Raghavachari, A. Rendell, J. C. Burant, S. S. Iyengar, J. Tomasi, M. Cossi, N. Rega, J. M. Millam, M. Klene, J. E., Knox, J. B. Cross, V. Bakken, C. Adamo, J. Jaramillo, R. Gomperts, R. E. Stratmann, O. Yazyev, A. J. Austin, R. Cammi, C. Pomelli, J. W. Ochterski, R. L. Martin, K. Morokuma, V. G. Zakrzewski, G. A. Voth, P. Salvador, J. J. Dannenberg, S. Dapprich, A. D. Daniels, Ö. Farkas, J. B. Foresman, J. V. Ortiz, J. Cioslowski, D. J. Fox, Gaussian Inc., Wallingford, CT (USA), 2009.
[50] D. A. Case, T. A. Darden, T. E. Cheatham, C. L. Simmerling, J. Wang, R. E. Duke, R. Luo, K. M. Merz, D. A. Pearlman, M. Crowley, R. C. Walker, W. Zhang, B. Wang, S. Hayik, A. Roitberg, G. Seabra, K. F. Wong, F. Paesani, X. Wu, S. Brozell, V. Tsui, H. Gohlke, L. Yang, C. Tan, J. Mongan, V. Hornak, G. Cui, P. Beroza, D. H. Mathews, C. Schafmeister, W. S. Ross, P. A. Kollman, AMBER 9, University of California, San Francisco, CA (USA), 2006.
[51] Y. Duan, C. Wu, S. Chowdhury, M. C. Lee, G. Xiong, W. Zhang, R. Yang, P. Cieplak, R. Luo, T. Lee, *J. Comput. Chem.* **2003**, *24*, 1999 – 2012.
[52] W. L. Jorgensen, J. Chandrasekhar, J. D. Madura, R. W. Impey, L. M. Klein, *J. Chem. Phys.* **1983**, *79*, 926 – 936.
[53] U. Essmann, L. Perera, M. L. Berkowitz, T. Darden, H. Lee, L. G. A. Pedersen, *J. Chem. Phys.* **1995**, *103*, 8577 – 8593.
[54] J. P. Ryckaert, G. Ciccotti, H. J. C. Berendsen, *J. Comput. Phys.* **1977**, *23*, 327 – 341.
[55] H. J. C. Berendsen, J. P. M. Postma, W. F. Van Gunsteren, A. Di Nola, J. R. Haak, *J. Chem. Phys.* **1984**, *81*, 3684 – 3690.
[56] N. A. Baker, D. Sept, S. Joseph, M. J. Holst, J. A. McCammon, *Proc. Natl. Acad. Sci. USA* **2001**, *98*, 10037 – 10041.

[57] D. Sitkoff, K. A. Sharp, B. Honing, *J. Phys. Chem.* **1994**, *98*, 1978 – 1988.
[58] P. Hazel, G. N. Parkinson, S. Neidle, *Nucleic Acids Res.* **2006**, *34*, 2117 – 2127.
[59] J. Kottalam, D. A. Case, *Biopolymers* **1990**, *29*, 1409 – 1421.
[60] W. Humphrey, A. Dalke, K. Schulten, *J. Mol. Graphics* **1996**,*14*, 27 – 28.
[61] C. F. Macrae, I. J. Bruno, J. A. Chisholm, P. R. Edgington, P. McCabe, E. Pidcock, L. Rodriguez-Monge, R. Taylor, J. van de Streek, P. A. Wood, *J. Appl. Crystallogr.* **2008**, *41*, 466 – 470.

Received: August 5, 2010
Revised: September 18, 2010
Published online on October 18, 2010

